EARTH SCIENCES

10.1126/sciadv.1501768

Experimental river delta size set by multiple floods and backwater hydrodynamics

Vamsi Ganti,*† Austin J. Chadwick, Hima J. Hassenruck-Gudipati,‡ Brian M. Fuller, Michael P. Lamb

River deltas worldwide are currently under threat of drowning and destruction by sea-level rise, subsidence, and oceanic storms, highlighting the need to quantify their growth processes. Deltas are built through construction of sediment lobes, and emerging theories suggest that the size of delta lobes scales with backwater hydrodynamics, but these ideas are difficult to test on natural deltas that evolve slowly. We show results of the first laboratory delta built through successive deposition of lobes that maintain a constant size. We show that the characteristic size of delta lobes emerges because of a preferential avulsion node—the location where the river course periodically and abruptly shifts—that remains fixed spatially relative to the prograding shoreline. The preferential avulsion node in our experiments is a consequence of multiple river floods and Froude-subcritical flows that produce persistent nonuniform flows and a peak in net channel deposition within the backwater zone of the coastal river. In contrast, experimental deltas without multiple floods produce flows with uniform velocities and delta lobes that lack a characteristic size. Results have broad applications to sustainable management of deltas and for decoding their stratigraphic record on Earth and Mars.

INTRODUCTION

Deltas are highly dynamic, often fan-shaped depositional systems that form when a river enters a basin of standing water (for example, ocean or lake). They are extremely resource-rich landscapes and host more than half a billion people (*1*, *2*). Many deltas are low-lying areas that are vulnerable to drowning and destruction by relative sea-level rise, oceanic storms, and reduction in upstream sediment supply owing to anthropogenic interference (*1*–*8*). Because deltas are net depositional landscapes, they contribute to the stratigraphic record and hold important information pertaining to past environments, as well as water and habitability on Earth and Mars (*8*–*11*). We need mechanistic theories of delta size for the sustainable management of these important landforms and for decoding their stratigraphic record.

Deltas grow at the largest scale through repeated cycles of delta lobe construction via deposition, followed by lobe abandonment by river avulsion—an abrupt shift in the river course (*12*–*14*). Lobe scale avulsions often occur regularly and around a persistent spatial node, leading to the characteristic delta-shaped planform morphology, and thus ultimately set the fundamental length scale of deltas [for example, (*14*)]. Whereas avulsion node locations on some steep fan deltas and alluvial fans are topographically controlled (for example, because of a change in confinement or bed slope at a canyon-fan transition) (*12*, *15*–*17*), avulsions on low-gradient rivers occur around a persistent spatial node but without any apparent change in bed slope or confinement (*15*). Instead, river avulsions on many low-gradient deltas occur at a characteristic distance upstream of the shoreline, known as the avulsion length (L_A), which scales to first order with the so-called backwater length of the alluvial river (*14*, *15*, *18*, *19*), although scatter of at least a factor of 2 is evident (Fig. 1; L_b). The backwater length of an alluvial river is a scale parameter for the length over which nonuniform (gradually varied) flow can exist as a result of disequilibrium between the river depth far upstream (normal-flow depth) and the river depth at the shoreline (fig. S1), which is forced in part through the boundary condition of sea level (*20*). The backwater length can be approximated roughly as the ratio of the characteristic flow depth (h_c) and the reach riverbed slope (*11*) (S) (that is, $L_b = h_c/S$) and can extend hundreds of kilometers upstream of the shoreline for large, low-sloping rivers [for example, (*14*, *18*, *20*, *21*)].

Recently, using a quasi–two-dimensional (2D) numerical model, Chatanantavet *et al.* (*18*) proposed that the avulsion location on river deltas scales with the backwater length because of a peak in in-channel sedimentation within the backwater zone that develops as a result of Froude-subcritical flows and floods of variable discharge, conditions that typify large, low-sloping deltaic rivers. In their simulations, small floods resulted in flow deceleration (fig. S1) and a downstream migrating wave of deposition that initiated near the upstream extent of the backwater reach. Large floods produced spatially accelerating flow in the backwater zone (fig. S1) and an upstream migrating wave of riverbed erosion that initiated near the river mouth. The net effect of multiple cycles of floods was persistent nonuniform flows and rates of in-channel sedimentation that peaked within the backwater zone. They also showed that modeled rivers under a constant flood discharge—a common assumption in other delta models and experiments (*22*–*29*)—had spatially uniform flow velocities and lacked a peak in in-channel sedimentation rates. Flume experiments confirm that sedimentation during constant discharge conditions tends to preferentially occur in zones of spatial flow deceleration, which reduces water depths, increases flow velocities, and eventually drives the river to a state of uniform flow velocities and uniform sedimentation patterns (*30*). These experiments also produced persistent nonuniform flow and persistent riverbed adjustment under conditions of multiple floods and subcritical flows (*30*); however, they did not produce avulsions or a delta built by successive cycles of lobe building and abandonment.

An important implication of this emerging theory for the scaling relationship between backwater length and delta lobe size is that avulsion location may be tied to backwater hydrodynamics only under cases

Division of Geological and Planetary Sciences, California Institute of Technology, 1200 East California Boulevard, Pasadena, CA 91125, USA.
*Present address: Department of Earth Science and Engineering, Imperial College London, South Kensington Campus, Exhibition Road, London SW7 2AZ, UK.
†Corresponding author. Email: v.ganti@imperial.ac.uk
‡Present address: Jackson School of Geosciences, University of Texas at Austin, Austin, TX 78712, USA.

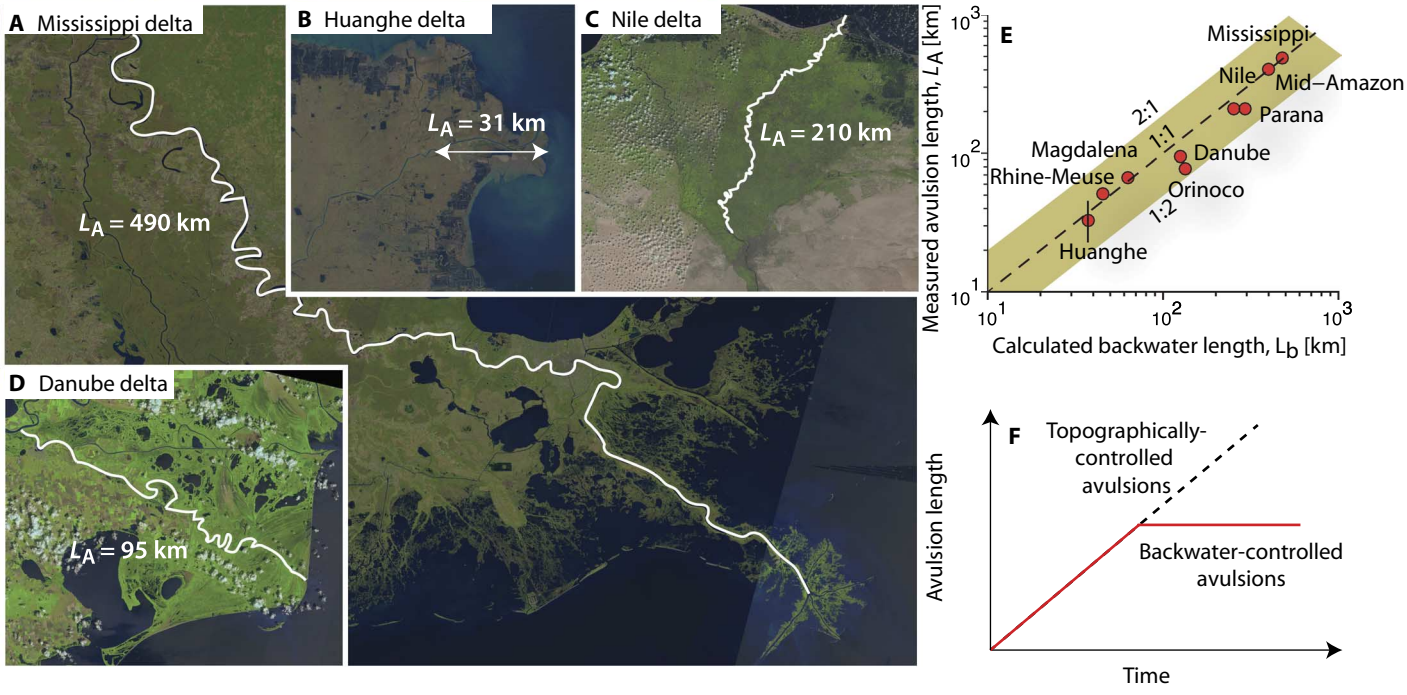

Fig. 1. Compilation of avulsion lengths on river deltas scales with the computed backwater length. (**A** to **D**) Satellite imagery showing measured avulsion length (L_A) for four deltaic systems. (**E**) Correlation between measured avulsion length and the computed backwater length (L_b) suggests that avulsions on deltas occur within the upstream portion of the backwater zone (the shaded region is bounded by 1:2 and 2:1 lines), which determines the length scale over which the alluvial river feels the downstream boundary condition of sea level (*14*, *15*, *18*). Data compilation of avulsion length and backwater length is from previously published work (*14*, *15*, *18*, *19*); see those works for methods. Because avulsion is fundamentally a stochastic process (*31*), the scaling relationship between backwater length and the avulsion length can be viewed to represent an average over multiple avulsion cycles (*14*). (**F**) Because backwater hydrodynamics arise as a result of the downstream boundary condition of sea level, backwater-controlled avulsion nodes should translate seaward in step with shoreline progradation such that avulsion length on deltas reaches a constant value in time. This is in contrast with topographically controlled avulsions, which are common to alluvial fans and fan deltas (*15*), where avulsions may occur at a change in confinement (for example, canyon-fan transition) and the avulsion length can grow in time without impedance.

of variable discharge floods that induce persistent bed adjustment (Fig. 1F). Thus, low-gradient deltas with backwater-controlled avulsions should maintain a constant lobe size during shoreline progradation because the backwater length is tied to the shoreline. In contrast, under constant discharge conditions, backwater hydrodynamics do not significantly influence deposition patterns, and avulsion locations may be topographically controlled, similar to alluvial fans or fan deltas, resulting in an avulsion length that can grow indefinitely (Fig. 1F). Testing this hypothesis in nature is difficult given that the time scale for avulsions on most deltas is hundreds to thousands of years (*31*). Furthermore, most previous deltaic experiments have been performed under constant discharge conditions (*22*–*26*) or supercritical flows that preclude backwater hydrodynamics (*32*). To fill this knowledge gap, we performed scaled physical experiments to grow a delta and observe its dynamics under conditions of subcritical flow and multiple floods. Similar to the work by Chatanantavet *et al.* (*18*), we compare these results to a control experiment that also had subcritical flow but, in this case, under constant discharge conditions.

RESULTS

The experimental arrangement consisted of a 7-cm-wide, 7-m-long alluvial river, which drained into an ocean basin (5 m × 3 m), building its own delta (Fig. 2). Experiments were conducted under subcritical flow conditions (Froude number: Fr < 1) allowing for backwater hydrodynamics, constant sea level, and used crushed walnut shells (ρ_s = 1300 kg/m^3) of uniform grain size (D = 0.7 mm) transported in bed load and intermittent suspension (Table 1; Materials and Methods). Previous experiments required highly cohesive sediment to produce single-thread channels and morphodynamic adjustment through backfilling and backwater-influenced avulsions (*22*). Here, we use sediment that lacks significant cohesion and, instead, focus on low Froude numbers and variable discharge floods, both intrinsic to any lowland river system, as drivers for transient morphodynamics.

Natural deltas can be affected by a wide range of processes that, by design, are not included in our experiments, including sea-level rise, subsidence, tides, waves, oceanic storms, density gradients, strongly cohesive sediment, and vegetation [for example, (*14*, *22*, *33*–*35*)]. These processes are neglected because many natural deltas across a wide range of environments and tectonic settings appear to scale to first order with only the backwater length of the feeder river (Fig. 1), a relationship that has yet to be demonstrated experimentally. Consequently, our experiments were designed to isolate the effects of floods and backwater hydrodynamics on delta lobe size in the simplest way possible.

We conducted two experiments. In the first experiment (experiment A), we held the water and sediment discharge to be constant, scaled approximately as an annual bankfull flood (Materials and Methods).

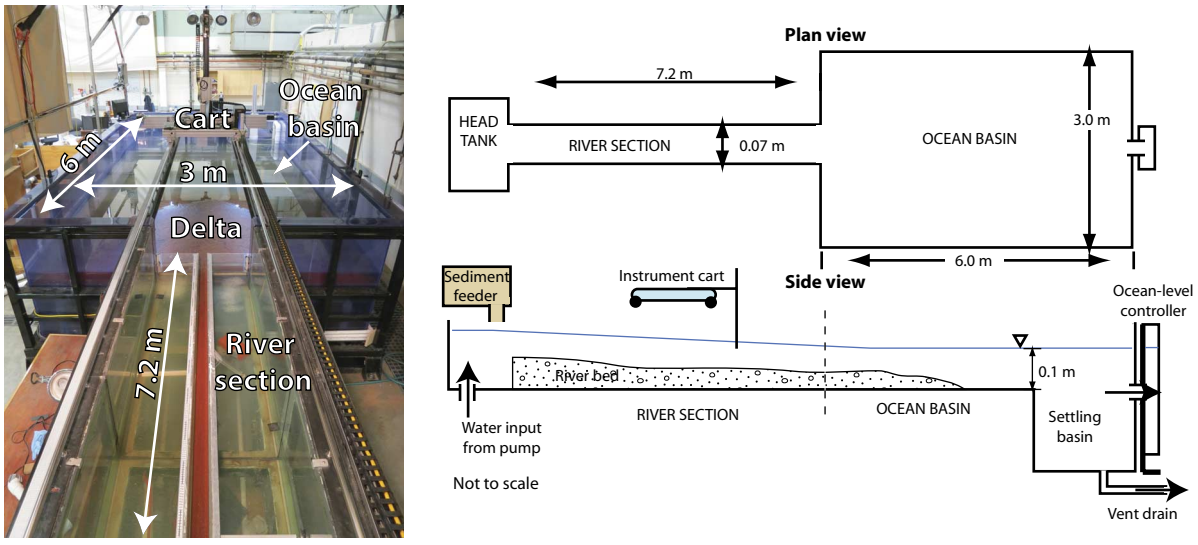

Fig. 2. Experimental arrangement at Caltech Earth Surface Dynamics Laboratory. Schematic of the experimental arrangement along with a perspective photograph showing the alluvial river section, ocean basin, and the instrument cart, which was used to collect water surface and bed elevation data during both experiments.

Table 1. The measured and given parameters of both the constant discharge and variable discharge deltas.

	Constant discharge experiment (experiment A)	Variable discharge experiment (experiment B)	
		Low flow (M1 event)	High flow (M2 event)
Water discharge, Q_w (liters/min)	8.3	8.3	12.0
Sediment feed, Q_s (g/min)	69	36	60
Run time	65 hours	40 min*	15 min*
Normal-flow depth†, h_n (mm)	8.5	9.5	13
Normal-flow Froude number†, Fr (–)	0.81	0.67	0.63
Channel bed slope†, S (–)	5.5×10^{-3}	3.3×10^{-3}	3.3×10^{-3}
Backwater length, L_b (m)	1.5‡	2.9	
Rouse number (–)	3.6	4.5	3.8
Number of avulsions	80	9	32

*The low- and high-flow events in experiment B were repeated 160 times, resulting in a total experimental run time of ~150 hours. †The normal-flow depth, normal-flow Froude number, and channel bed slope were averaged over the first 3 m of the experimental river, which was within the normal-flow zone in both experiments. See figs. S2 and S3 for additional details. ‡Although we can compute the backwater length scale in experiment A as a scale parameter, we note that this does not imply that nonuniform flow persisted over these length scales in our experiment (see figs. S2 and S6).

Avulsions in this experiment are expected to be topographically controlled by the change in confinement between the fixed-width section of our river channel and the ocean basin ($x = 0.4$ in fig. S2), and therefore, the avulsion length is expected to grow in time (Fig. 1F). In the second experiment (experiment B), we alternated between 40-min duration low flows and 15-min high flows, scaled roughly as a bankfull flood, and a larger 30-year recurrence interval flood (Materials and Methods), 160 times under constant sea level and subcritical flow conditions (Materials and Methods; fig. S3). Avulsions in this experiment are expected to scale with the backwater length (Fig. 1F). In experiment B, the sediment supply was adjusted commensurate with the water discharge for the high- and low-flow flood events to maintain a constant self-formed bed slope in the upstream normal-flow reach (Materials and Methods). This ensured that the patterns of erosion and deposition in the experiment were due to backwater effects rather than imbalances in the imposed sediment and water discharges (Materials and Methods). Further, the duration of high and low flows in experiment B was designed to be short enough such that the bed within the backwater zone was in a state of transient adjustment due to in-channel sedimentation or erosion from previous flood event. This was argued previously to be necessary to produce backwater-controlled avulsions (*18*). Overhead images of deltaic evolution were collected every minute and used to identify the

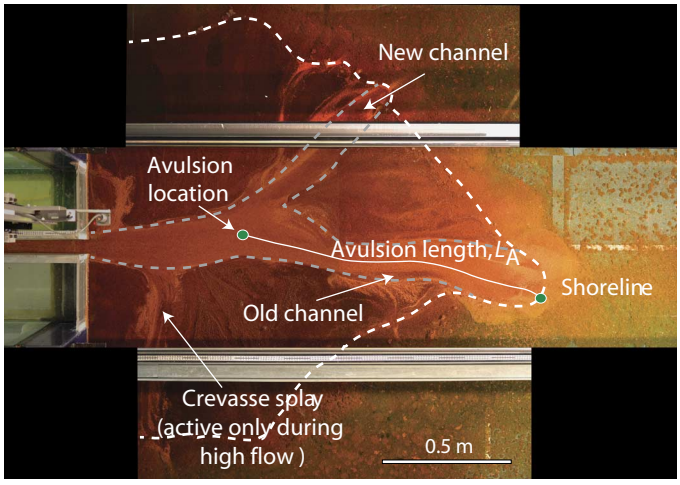

Fig. 3. Overhead image of an avulsion during the variable discharge experiment. The image shows the location of river avulsion, old and new channels, river mouth, and crevasse splays, which were active only during the high-flow events. The avulsion length was measured along the channel thalweg and normalized by the backwater length of the low flow (Table 1). The two silver horizontal bars are instrument rails that sit above the experiment. The gray and white dashed lines indicate the channel banks and the shoreline, respectively.

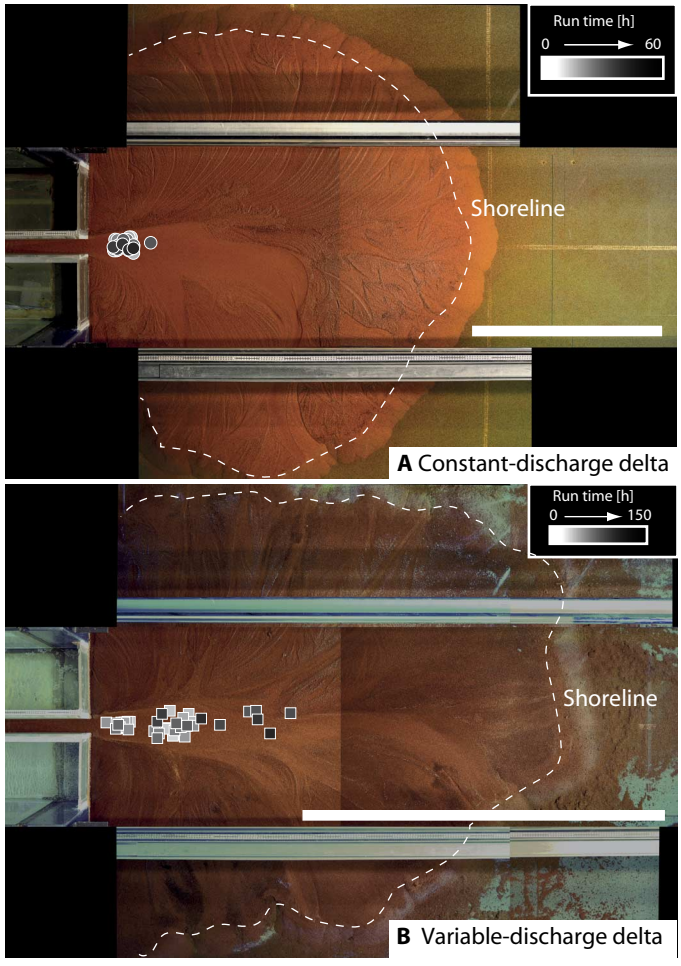

Fig. 4. Comparison of avulsion sites for constant discharge delta versus the variable discharge delta. (**A** and **B**) Avulsion sites through time for (A) experiment A and (B) experiment B overlain on the photographs of the deltas at the end of their experimental runs. The colors of the avulsion sites are graded from white to black in time, and the shorelines are indicated as dashed white lines. The white scale bars indicate a length of $0.5L_b$, which are 0.75 and 1.45 m for experiments A and B (Table 1), respectively.

location of avulsions, the shoreline, and the distance between the two (that is, L_A) (Fig. 3 and fig. S4; Materials and Methods). Avulsions were defined as abrupt and permanent changes in the course of the river that captured the majority of water flow and resulted in the construction of a new sediment lobe. Avulsions were accompanied by abrupt abandonment of the old channel in both experiments; however, gradual abandonment occurred in experiment B during some avulsion cycles. Smaller channel breaches that did not satisfy these criteria were classified as crevasse splays [for example, (*12*)]. Both experiments produced deltas that grew through several tens of cycles of avulsion and lobe construction (Table 1).

Results show that the avulsions in experiment A were tied to the tank boundary (Fig. 4A, fig. S5, and movie S1) and the delta grew in time because of shoreline progradation, similar to previous experiments that lacked persistent backwater hydrodynamics [for example, (*36*)]. Thus, subcritical flow alone is not sufficient to produce avulsions that scale with the backwater length. This is in contrast to experiment B, where avulsions initially occurred at the tank boundary; however, as the delta grew bigger, the avulsion sites translated seaward with shoreline progradation (Fig. 4B and movie S2). Multiple floods in experiment B also produced a delta that was significantly more lobate in planform (Fig. 4). Figure 5 shows the evolution of the ratio of the avulsion length (L_A) to the backwater length (L_b) as a function of dimensionless time. Owing to different average sediment fluxes in the two experiments (Table 1), we normalized the experimental run time by the time it would take to create a radially symmetric, semicircular delta of size $0.5L_b$ for comparison (Materials and Methods). Results demonstrate that in experiment B, the avulsion sites were tied to the tank boundary until the delta reached a size of ~$0.5L_b$ (dimensionless time of 1 in Fig. 5), beyond which the avulsion sites translated seaward in step with shoreline progradation, thus maintaining deltaic lobes of constant size (Figs. 4B and 5). Thus, the combination of subcritical flow and multiple floods in experiment B produced avulsions that scaled with the backwater length.

Why do avulsions preferentially occur at a location that maintains a consistent distance upstream of the shoreline and scales with the backwater length? The process of river avulsion has two fundamental requirements. First, focused in-channel aggradation at a particular location, which is referred to as the process of avulsion "setup," makes the river poised for an avulsion (*12*, *37*). The avulsion "trigger" is typically an event whereby water flow leaves the channel and/or where erosion induces levee breach during floods (*38*–*40*). Our experiments show that persistent backwater and drawdown hydrodynamics significantly affect the process of avulsion setup and that this is controlling avulsion location in our experiments, as described below.

Using measurements of bed topography during the experiments (Materials and Methods), we tracked the in-channel sedimentation that occurred along the centerline of the river during each flood event (that

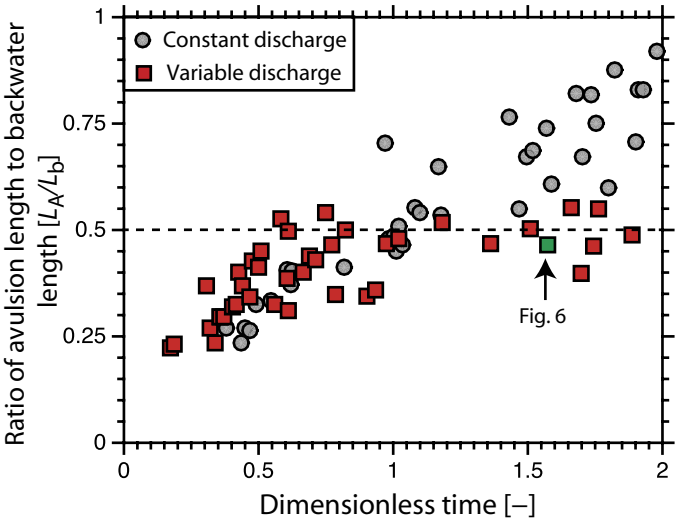

Fig. 5. Avulsion sites translate seaward in step with shoreline progradation, thus maintaining a constant delta lobe size parameterized here as the ratio of the avulsion length (L_A) to the backwater length (L_b). Plot showing the evolution of the ratio of the avulsion length to the backwater length as a function of dimensionless time, where the experimental run time was normalized by the time it takes to build a radially symmetric, semicircular delta of size $0.5L_b$ (Materials and Methods). In experiment B, the avulsion sites translate seaward in step with shoreline progradation, maintaining an avulsion length of approximately $0.5L_b$. Detailed measurements of water and bed surface elevation profiles, flow velocities, and in-channel sedimentation are shown for the avulsion indicated by the green marker in Fig. 6.

is, each low-flow and high-flow event, where the duration of each flow is referred to as an "event") and also during a whole avulsion cycle (that is, from when a new channel was formed until it avulsed to a new location). During our low-flow events, we observed deceleration of the flow in the backwater zone (Fig. 6B), which produced deposition in the middle of the backwater zone (Fig. 6C). In contrast, during our high-flow events, the water surface slope steepened (Fig. 6A), and flow accelerated within $0.3L_b$ of the shoreline, which produced erosion. On average, a peak in deposition from low flows occurred at ~$0.35L_b$ from the shoreline (Fig. 6C), a peak in erosion from high flows occurred at ~$0.25L_b$ from the shoreline, and, together, all events summed to produce enhanced in-channel sedimentation at ~$0.40L_b$ from the shoreline (Fig. 6C), which is coincident with the eventual avulsion that occurred at ~$0.45L_b$ (Fig. 5). Ultimately, backwater hydrodynamics and deposition occurred during low flow as a result of the overdeepened channel from the preceding high flow, and erosion occurred during high flow because of deposition and channel shallowing from the previous low flow. Erosion and deposition from successive events did not balance because deposition was enhanced in the upstream part of the backwater zone, and erosion in the downstream part. Thus, when summed over multiple flow events during an avulsion cycle, successive alternation of low- and high-flow events produced a pattern of in-channel sedimentation that peaked within the middle of the backwater zone, similar to recent theory (*18*). In contrast, for the constant discharge case within the backwater zone, we observed no spatial changes in water surface slope, no systematic flow acceleration or deceleration (fig. S6), and, consequently, an avulsion node that remained tied to the tank boundary and did not scale with the backwater length (Figs. 4A and 5).

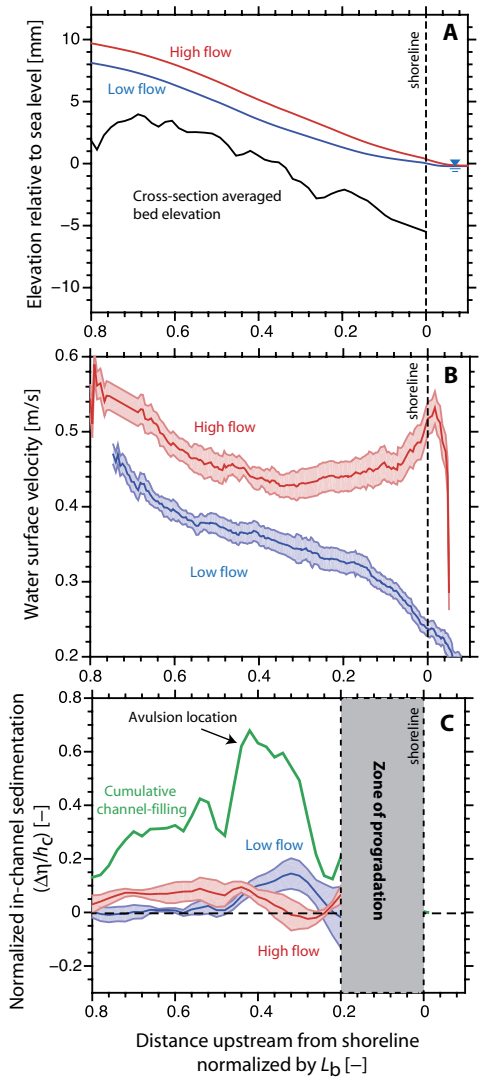

Fig. 6. Competition between low-flow deposition and high-flow erosion results in an in-channel sedimentation peak at the avulsion site, which scales with the backwater length. (**A**) Instantaneous water and bed surface elevation (black curve) profiles during low flow (blue curve) and high flow (red curve) as a function of streamwise distance from the shoreline, normalized by L_b at the beginning of the avulsion cycle (Materials and Methods). (**B**) During low flow, the flow decelerates in the backwater reach; however, during high flow, the water surface slope steepens, and flow accelerates through the lowermost portion of the backwater zone. (**C**) In-channel sedimentation ($\Delta\eta$) normalized by the normal-flow depth of low flow (h_c) measured during each flow event of the avulsion cycle (red and blue lines indicate high- and low-flow events, respectively, and the shaded region is the SE from averaging over multiple flow events). Over multiple flow events during this avulsion cycle (six low-flow and five high-flow events), the competition between low-flow deposition and high-flow erosion results in an in-channel sedimentation peak within the backwater reach (~0.40 L_b), near where the eventual avulsion occurred (~0.45 L_b for avulsion location). The upstream distance was measured from the final shoreline when the avulsion occurred, and in-channel sedimentation data are not plotted for abscissae < 0.2 because this is a zone of progradation during the avulsion cycle, which precludes measurements of vertical aggradation. The upstream extent of these plots corresponds to the location where the river exits the narrow section in our experimental facility.

DISCUSSION AND CONCLUSIONS

Our work provides a mechanistic underpinning of the observed correlation between avulsion length and backwater length on lowland river deltas (*14*, *15*, *18*, *19*). Our results highlight the legacy of the transient nature of sediment erosion caused during flood events in determining the fundamental length scale of deltas. Unlike rivers upstream of the backwater zone, which can be characterized by a single characteristic flood discharge that is responsible for the most geomorphic work (*41*, *42*), the fundamental scale of deltas emerges only under conditions of perpetual transient morphodynamic adjustment. Subcritical flows and multiple floods of variable discharge allow nonuniform flow and nonuniform patterns of in-channel sedimentation to persist in coastal rivers, which ultimately leads to a preferred avulsion location within the backwater zone. In contrast, constant discharge flows, even under subcritical flow, tend toward uniform-flow conditions with no morphodynamic signature of backwater hydrodynamics. Thus, multiple floods and Froude-subcritical flows are the two necessary conditions to produce avulsions that scale with the backwater length in our experiments.

In addition to river floods, persistent bed adjustment in natural deltas may occur by other mechanisms, including rapid lobe progradation, mouth bar deposition (*22*), or relative sea-level rise, which might produce avulsions that scale differently than $L_A \sim 0.5L_b$ [for example, (*18*)]. In addition to backwater hydrodynamics, waves, tides, vegetation, and significant sediment cohesion play important roles in delta evolution [for example, (*34*, *35*)]. These processes may help to explain some of the variability in the ratio of L_A/L_b as observed in natural deltas (Fig. 1). Independent of backwater hydrodynamics, avulsions can also be driven by topographic controls, as on alluvial fans and fan deltas (and in our experiment A), by lateral gradients in subsidence rates [for example, (*33*)], and can occur in river channels far upstream of deltas [for example, (*12*, *31*)], making it important to distinguish backwater-controlled avulsions from other mechanisms (*15*).

Because river avulsions occur infrequently in natural systems, field observations of avulsion site translation are rare. However, the Huanghe, China, which before major engineering (1936) avulsed on an unprecedented decadal time scale, is an important example of backwater-controlled avulsion sites that translated seaward in step with shoreline progradation (*15*). In our experiments, as on the Huanghe, the seaward translation of the avulsion sites leaves behind part of the deltaic plain, which no longer receives sediment and water through major river avulsions. In our experiment, these parts of the deltaic plain were nourished with sediment through persistent levee-breaching crevasse splays and overbank deposition during high-flow events (Fig. 3). For natural deltas, minor avulsions, distributary networks, cohesive washload sediment, and vegetation [for example, (*12*, *43*)] may also help promote aggradation on the relict deltaic plain.

Our experiments were conducted under no externally imposed subsidence or sea-level rise, such that seaward shoreline migration was due to delta deposition alone. In natural deltas, subsidence, sea-level rise, and reduced sediment supply due to bank stabilization and dams can all act to stall or reverse the direction of shoreline migration, a problem on many deltas worldwide (*1*). Our experimental results suggest that the avulsion node should shift inland on drowning deltas with retreating shorelines, increasing the hazard of avulsions to upstream communities. In addition to shoreline migration, numerical models indicate that the avulsion node location may move further inland, relative to the backwater length (for example, $L_A = 1$ to $2\ L_b$) under cases of significant relative sea-level rise (*18*), exacerbating the problem. The backwater length scaling of delta lobe size provides a quantitative expectation for the most likely location of future avulsions, which can be used in management strategies for engineered diversions on deltas to mitigate land loss (*44*).

These results also bolster the use of backwater length as a paleohydraulic reconstruction tool (*9*), where delta lobe size, flow depth, and bed slope are related, that is, $L_A \sim L_b = h_c/S$, and progressive avulsion node translation provides a tool for differentiating alluvial fan deposits from deltaic deposits, in which the latter have implications for long-lived lakes and oceans on other planetary bodies such as Mars and Titan. Although the backwater length scale sets the limiting size of deltaic lobes (Fig. 5), this size may not always be attained. For example, in cases of high subsidence rates and when the feeder river channel is bounded by a canyon, the deltaic lobes may never become large enough to have backwater-controlled avulsions, akin to avulsions observed during the early phase of deltaic growth in our experiment B (Fig. 5).

On long geologic time scales, mass balance between the input sediment supply and the accommodation created by subsidence and relative sea-level rise likely dictate the scale over which delta deposits can be preserved in the stratigraphic record (*26*, *45*, *46*), that is, $L_{mass} \sim q_s/\sigma$, where L_{mass} is a "mass-balance" length scale, q_s is the input fluvial sediment flux per unit width, and σ is the rate of subsidence and relative sea-level rise. In the limiting case of $L_{mass} >> L_b$, the backwater-controlled avulsion node is likely to be well within the zone of the subsidence, indicating that the dynamics of deltaic evolution and the coastal plain upstream of the avulsion node may be preserved in the sedimentary record. In contrast, if $L_{mass} << L_b$, then the backwater-controlled avulsion node of the delta is likely to be upstream of the zone of the subsidence, indicating that only the portion of the delta within the subsidence zone may be preserved in the sedimentary record. Our experimental results suggest that the stratigraphic architecture of deltaic deposits is likely composed of 3D amalgamated lobes of similar scale (*47*), set by a spatially shifting avulsion node as the delta progrades basinward (*15*). This is in contrast to the Gilbert-type models that define distinct topset and foreset stratigraphy in a largely 2D framework [for example, (*48*, *49*)]. Ultimately, the backwater length, which sets the dominant length scale of river deltas, is the fundamental building block of fluvio-deltaic stratigraphy, with implications that span reservoir geology to paleoenvironmental reconstruction of ancient Earth and Mars.

MATERIALS AND METHODS

Experimental arrangement and design

The experiments were conducted with fresh water in the river-ocean facility at the Caltech Earth Surface Dynamics Laboratory. The experimental arrangement consisted of a 7-cm-wide, 7-m-long alluvial river, which drained into an "ocean" basin (5 m × 3 m) with 10-cm-deep standing water (Fig. 2). Sediment and water were fed at the upstream end of the alluvial river, and the sea level was held constant during the experiments using a programmable standpipe at the downstream end of the ocean basin. Two experiments were conducted, with each experiment starting with no sediment in the ocean basin. In the first experiment (experiment A), sediment and water were fed at a constant rate, and the alluvial river was allowed to build its own delta through time. In contrast, in the second experiment (experiment B), we oscillated between a 40-min low flow and 15-min high flow for 160 cycles,

such that the delta grew under persistent backwater and drawdown hydrodynamics. With a quasi-2D, coupled hydrodynamic and morphodynamic model as a guide (*18*, *20*, *30*), the experimental water and sediment discharge in experiment B were set such that both discharge events created an equivalent bed slope for normal-flow conditions in which sediment transport was at capacity—an important aspect of our experiments considering that imbalances in sediment supply and water discharge in itself can cause adjustment of the equilibrium bed slope (*50*). The discharge events were chosen to produce backwater hydrodynamics and deposition during low flow (that is, M1 regime) and drawdown and erosion during high flow (that is, M2 regime) (*20*, *30*, *51*). In addition to achieving backwater and drawdown dynamics, the water and sediment fluxes were chosen such that the experiments produced subcritical flows, relatively low bed slopes (typical of large natural deltas), relatively small backwater lengths, and measurable changes between the flow depths for low flow and high flow, respectively (Table 1). For the constant discharge experiment, the flow discharge was chosen to be equal to the low-flow conditions of the variable discharge experiment; however, we increased the sediment infeed rate relative to experiment B to speed up the deltaic evolution, maintaining the subcritical flow conditions (Table 1 and fig. S2). To achieve the correct scaling of flow velocity (Fr number scaling), bed slope, and backwater length, we needed a relatively long alluvial river section (7 m; Fig. 2), such that water and sediment were fed at the upstream end, which is well within the normal-flow reach of the alluvial river.

Figures S2 and S3 show the instantaneous water surface and bed surface profiles along with the computed Froude numbers and the measured flow depths during both experiments, which highlight the subcritical flow conditions in both experiments. We achieved the Froude number scaling in our experiments in part by using crushed walnut shells of uniform grain diameter (D = 0.7 mm) as the sediment. Because crushed walnut shells (ρ_s = 1300 kg/m^3) are significantly lighter than sand (ρ_s = 2700 kg/m^3), flows with relatively low velocities mobilized sediment, resulting in sediment transport and deltaic evolution. During our experiments, sediment transport primarily occurred as bed load with some suspension during the high-flow conditions. The computed Rouse numbers ($P = {}^{w_s}/\kappa u_*$), where w_s = 32 mm/s is the settling velocity of the sediment [calculated by Chatanantavet and Lamb (*30*)], u_* is the shear velocity [computed as $(gh_nS)^{1/2}$, where g is the gravitational acceleration, h_n is the normal-flow depth, and S is the bed slope], and κ = 0.41 is the von Karman constant, were 4.5 and 3.8 for low flow and high flow, respectively, and 3.6 for the constant discharge experiment (Table 1). The bed was mostly planar, and no form drag correction was performed. All our experiments fell within the range of intermittent suspension (P < 6.1 for large-particle Reynolds numbers) (*52*).

Although our experiment B was not scaled to any natural delta, it is useful to cast our flow variability in light of natural flow variability on deltas. For example, if we were to treat our low flow as a bankfull discharge (flood event with recurrence interval of 2 years) on the Mississippi delta, then the high flow would correspond to a flood event with a recurrence interval of ~30 years based on the normal-flow depths of the two events in our experiments [for example, (*20*)]. In this framework, experiment A would correspond to a delta that evolved under constant bankfull discharge conditions. The duration of each flow in experiment B was long enough such that significant deposition or erosion occurred during each flow event but short enough to prevent the bed from reaching morphodynamic equilibrium with that flood event. This not only allows for the persistence of transient backwater hydrodynamics but also forces the experimental alluvial river to be in a state of perpetual disequilibrium, which has been argued to be the case for most natural coastal rivers (*30*). Thus, the key difference between our experiments A and B was that experiment A did not have persistent backwater and drawdown hydrodynamics; in the absence of multiple flood events, the bed in experiment A aggraded such that near-normal-flow conditions with uniform water velocities existed everywhere (fig. S6). Thus, subcritical flow is a necessary, but not sufficient, condition to produce long-lived gradually varied flow; in addition, the flow depth must deviate from the normal-flow depth, which in experiment B occurred through the action of multiple floods of different discharge. The similarity between our experiment A and alluvial fans and fan deltas is drawn because, in the absence of persistent backwater hydrodynamics, the avulsions in experiment A were driven by the change in confinement alone, which has been argued to be the primary mechanism for initiating avulsions on fans and fan deltas [for example, (*15*)].

Data collected

An ultrasound distance meter (Massa) and a laser triangulation sensor (Keyence) were mounted on a motorized 3D positioning instrument cart with submillimeter positioning accuracy. The ultrasound probe was used to measure the water surface elevation during experiments, and the laser sensor was used to measure bed topography when the flow was switched off. We collected water surface elevation twice during each flow event in experiment B—once each at the beginning and end of the flow event. Bed surface elevation of the long profile of the channel was collected along with the water surface elevation during the flow, which was later empirically corrected for the refraction index of light in water. Errors associated with both the index-of-refraction correction and instrument error are ±0.1 mm in the vertical dimension. In experiment B, water flow was switched off at the end of each flow event, and bed surface elevation data were collected for the whole delta. This procedure allowed us to evaluate the amount of bed elevation change that occurred during each flow event. In experiment A, similar measurements were made at irregular intervals throughout the experiment.

Six cameras were mounted on the frame bordering the experimental facility (Fig. 2), whose viewing area covered the whole deltaic plain (Figs. 3 and 4 and movies S1 and S2). These cameras simultaneously captured overhead images of the deltaic evolution at a temporal resolution of 1 min for the whole duration of the experiments. Multiple orthogonal tape measures were laid down on the ocean basin floor, and when the basin was dry, cameras were used to capture overhead images, which were used to calibrate the concatenation of the six images from these multiple cameras. During each flow event, a fluorescent dye pulse was introduced just upstream of the tank boundary, and the dye transport was captured using overhead videos at a rate of 59 frames per second (fps) (movie S3). These dye videos were then used for estimating the water surface velocity through the backwater reach for both experiments.

Table 1 summarizes the measured and given parameters for experiments A and B. The water discharge was directly measured during the experiments using an inline flow meter, whereas the sediment discharge was measured using a sediment hopper that was calibrated using a balance and stopwatch. The normal-flow depth (h_n) was computed by differencing the bed elevation and water elevation data from the narrow section within the normal-flow reach of the experimental river (averaged over the first 3 m of the narrow section over the duration of the experiment). The normal-flow Froude number was computed as follows: $\mathrm{Fr} = U/\sqrt{gh_n}$, where g is the gravitational

acceleration and U is the depth-averaged flow velocity. The depth-averaged flow velocity within the normal-flow reach of the alluvial river was computed by the ratio of the input water discharge and the product of the channel width (7 cm) and depth of flow (h_n). Note that the depth-averaged flow velocity is always less than the water surface velocity reported using dye videos in Fig. 6B and fig. S6.

Data processing

The bed elevation and water surface elevation data were filtered, where spurious spikes were removed through a spatial slope threshold (~2% of the data). Because our refraction index correction of the laser scans for submerged bed works only for standing-water case, we did not use the bed elevation measurements collected during the flow events. Instead, bed elevation measurements at the end of each flow event were used to characterize the patterns of deposition and erosion that occurred during each event. Further, anomalous data points whose elevation was lower than the ocean basin floor were removed (<1% of data). To denoise the data, we applied a moving-median filter with a kernel size of 1.5 cm to both the bed and water surface profiles. These methods were used for processing the 3D scans of the delta surface at the end of each flow event. Finally, the data removed during the filtering procedure were replaced using linear interpolation.

Definition of an avulsion in experiments

We identified both the avulsion locations and the shorelines on the concatenated images of deltaic evolution whose pixel coordinates were transformed into the coordinates of the instrument cart following calibration using tape measures. For experiment B, we defined an avulsion as the development of a new channel where the daughter (new) channel captured flow even during low-flow events along with the parent channel being partially or completely abandoned. This definition precludes the characterization of crevasse splays as avulsion events in our experiment. Crevasse splays were common during high-flow events that resulted in overbank flooding and channelization on the floodplain; however, splays were not active during low-flow events. In experiment A, crevasse splays were uncommon and avulsions were defined by the creation of the new channel. Channel abandonment was abrupt in experiment A.

Estimation of the avulsion length through time

We computed the avulsion lengths through time using the overhead images of the deltaic evolution during both experiments. The concatenated photograph, which corresponds to each avulsion, was first identified, and the pixel coordinates of the avulsion site and the river mouth were extracted (Fig. 3). The avulsion site was defined as the location of the levee breach that resulted in formation of a new channel (Fig. 3 and fig. S4). Because we defined the avulsion site as a point, the error associated with the calculation of the avulsion length can be a maximum of the channel widths, which were, on an average, 10 and 25 cm for experiments A and B at the location of the avulsion sites, respectively. This corresponds to an overall error of approximately $0.06L_b$ and $0.08L_b$ for experiments A and B, respectively. We note that this error is a maximum and the actual error should be less than this value for all the computed avulsion lengths (for example, fig. S4). We then measured the streamwise distance of the avulsion site from the river mouth, that is, the shoreline, to quantify the avulsion length for each avulsion cycle in both experiments. We converted the time stamp on each of the avulsion pictures into an experimental run time. We normalized the experimental run time with the time it would take to build a radially symmetric, semicircular delta of size $0.5L_b$ (T_{delta})

$$T_{delta} = \frac{\pi L_b^2 h_{ocean} \rho_s}{8 Q_s} \quad (1)$$

where h_{ocean} = 10 cm is the depth of water in the ocean basin, ρ_s is the density of crushed walnut shells, and Q_s is the sediment mass feed rate for each experiment (Table 1). This procedure allowed us to account for differences in the delta growth rate that were simply due to differences in the sediment feed rates between the experiments and, consequently, directly compare the location of avulsions across the experiments (Fig. 5).

Estimation of the in-channel sedimentation through an avulsion cycle

We used the bed topography data collected at the end of each flow event to estimate the amount of in-channel sedimentation during each flow event and through an avulsion cycle. Using the overhead images and dye videos of the delta as a guide, we first traced the river channel thalweg on the topography data and extracted the bed elevation perpendicular to the thalweg to get the channel cross-section topography at a spatial resolution of 1 cm. We then computed the cross-section averaged riverbed elevation at each location along the channel by estimating the cross-sectional area and evaluating the depth of the rectangular channel with the same width and area as the computed cross-sectional area. This procedure allowed us to account for the width changes in the channel during each flow. We then measured the vertical change in the cross-section averaged bed elevation through each flow event (that is, during low- and high-flow events) and also during an avulsion cycle, which was defined as the time from which a new channel was formed until it avulsed to a new location. The red and blue lines in Fig. 6C show the amount of in-channel sedimentation that occurred during each high- and low-flow event during the avulsion cycle, and the green curve shows the in-channel sedimentation that occurred through the whole avulsion cycle. The in-channel sedimentation during an avulsion cycle results from the combination of in-channel sedimentation from multiple low- and high-flow events during the avulsion cycle. The avulsion cycle shown in Fig. 6 was composed of six low-flow and five high-flow events, and the avulsion occurred during the sixth high-flow event. The shaded red and blue colors in Fig. 6C show the standard error (SE) in normalized in-channel sedimentation across high- and low-flow events, respectively. Thus, the green line in Fig. 6C is a summation of in-channel sedimentation that occurred during six low-flow and five high-flow events, whose average values along with SE are shown by blue and red curves, respectively.

Computation of water surface velocity using dye videos

We used the overhead dye videos (frame rate of 59 fps) to compute the water surface velocity on the deltaic plain in both experiments (movie S3). For each dye video, we used the color contrast between the dye (fluorescent) and the deltaic surface (brown) to automatically identify the location of the dye in each frame of the video. Each frame was then converted into a binary matrix of "dye" and "no dye," and we manually kept track of the location of the dye front in each frame of the video. Once the dye front was located, we estimated the distance traveled by the dye along the channel thalweg in successive frames and converted this computed distance into instantaneous surface velocity

using central differencing. Finally, the instantaneous surface velocity data were smoothed using a moving-window average filter over nonoverlapping windows of size 25 cm to produce Fig. 6B and fig. S6. The shaded region in these figures corresponds to the SE resulting from the spatial averaging. The water surface velocity computed using the dye videos is higher than the depth-averaged flow velocity, as expected.

SUPPLEMENTARY MATERIALS

Supplementary material for this article is available at http://advances.sciencemag.org/cgi/content/full/2/5/e1501768/DC1

Supplementary Materials and Methods

fig. S1. Idealized schematic of backwater and drawdown hydrodynamics.

fig. S2. Instantaneous measurements of water and bed surface profiles along with the measured flow depth, depth-averaged flow velocity, and Froude number for experiment A.

fig. S3. Instantaneous measurements of water and bed surface profiles along with the measured flow depth, depth-averaged flow velocity, and Froude number for both flows in experiment B.

fig. S4. Photo sequence of the process of avulsion in experiment B.

fig. S5. Temporal evolution of avulsion length in constant discharge delta.

fig. S6. Water surface velocity across the backwater reach in constant discharge delta.

table S1. Field data compilation of avulsion length and backwater length.

movie S1. Experimental evolution of constant discharge delta.

movie S2. Experimental evolution of variable discharge delta.

movie S3. Overhead dye video of the constant discharge delta.

References (*53*, *54*)

REFERENCES AND NOTES

1. J. P. M. Syvitski, A. J. Kettner, I. Overeem, E. W. H. Hutton, M. T. Hannon, G. R. Brakenridge, J. Day, C. Vörösmarty, Y. Saito, L. Giosan, R. J. Nicholls, Sinking deltas due to human activities. *Nat. Geosci.* **2**, 681–686 (2009).
2. C. J. Vörösmarty, J. Syvitski, J. Day, A. de Sherbinin, L. Giosan, C. Paola, Battling to save the world's river deltas. *Bull. At. Sci.* **65**, 31–43 (2009).
3. M. D. Blum, H. H. Roberts, Drowning of the Mississippi delta due to insufficient sediment supply and global sea-level rise. *Nat. Geosci.* **2**, 488–491 (2009).
4. J. P. M. Syvitski, Y. Saito, Morphodynamics of deltas under the influence of humans. *Global Planet. Change* **57**, 261–282 (2007).
5. J. P. M. Syvitski, C. J. Vörösmarty, A. J. Kettner, P. Green, Impact of humans on the flux of terrestrial sediment to the global coastal ocean. *Science* **308**, 376–380 (2005).
6. M. Meybeck, C. J. Vörösmarty, Fluvial filtering of land-to-ocean fluxes: From natural Holocene variations to Anthropocene. *C. R. Geosci.* **337**, 107–123 (2005).
7. Z. D. Tessler, C. J. Vörösmarty, M. Grossberg, I. Gladkova, H. Aizenman, J. P. M. Syvitski, E. Foufoula-Georgiou, Profiling risk and sustainability in coastal deltas of the world. *Science* **349**, 638–643 (2015).
8. T. S. Bianchi, M. A. Allison, Large-river delta-front estuaries as natural "recorders" of global environmental change. *Proc. Natl. Acad. Sci. U.S.A.* **106**, 8085–8092 (2009).
9. R. A. DiBiase, A. B. Limaye, J. S. Scheingross, W. W. Fischer, M. P. Lamb, Deltaic deposits at Aeolis Dorsa: Sedimentary evidence for a standing body of water in the northern plains of Mars. *J. Geophys. Res.* **118**, 1285–1302 (2013).
10. M. G. Kleinhans, Flow discharge and sediment transport models for estimating a minimum timescale of hydrological activity and channel and delta formation on Mars. *J. Geophys. Res.* **110**, E12003 (2005).
11. C. Paola, Quantitative models of sedimentary basin filling. *Sedimentology* **47**, 121–178 (2000).
12. R. Slingerland, N. D. Smith, River avulsions and their deposits. *Annu. Rev. Earth Planet. Sci.* **32**, 257–285 (2004).
13. J. R. L. Allen, A review of the origin and characteristics of recent alluvial sediments. *Sedimentology* **5**, 89–191 (1965).
14. D. J. Jerolmack, Conceptual framework for assessing the response of delta channel networks to Holocene sea level rise. *Quat. Sci. Rev.* **28**, 1786–1800 (2009).
15. V. Ganti, Z. Chu, M. P. Lamb, J. A. Nittrouer, G. Parker, Testing morphodynamic controls on the location and frequency of river avulsions on fans versus deltas: Huanghe (Yellow River), China. *Geophys. Res. Lett.* **41**, 7882–7890 (2014).
16. T. C. Blair, J. G. McPherson, Alluvial fans and their natural distinction from rivers based on morphology, hydraulic processes, sedimentary processes, and facies assemblages. *J. Sediment. Res.* **64A**, 450–489 (1994).
17. L. S. Jones, S. A. Schumm, in *Fluvial Sedimentology VI (Special Publication of the International Association of Sedimentologists)*, N. D. Smith, J. Rogers, Eds. (Blackwell, Oxford, 1999), vol. 28, pp. 171–178.
18. P. Chatanantavet, M. P. Lamb, J. A. Nittrouer, Backwater controls of avulsion location on deltas. *Geophys. Res. Lett.* **39**, L01402 (2012).
19. D. J. Jerolmack, J. B. Swenson, Scaling relationships and evolution of distributary networks on wave-influenced deltas. *Geophys. Res. Lett.* **34**, L23402 (2007).
20. M. P. Lamb, J. A. Nittrouer, D. Mohrig, J. Shaw, Backwater and river plume controls on scour upstream of river mouths: Implications for fluvio-deltaic morphodynamics. *J. Geophys. Res.* **117**, F01002 (2012).
21. J. A. Nittrouer, J. Shaw, M. P. Lamb, D. Mohrig, Spatial and temporal trends for water-flow velocity and bed-material transport in the lower Mississippi River. *Geol. Soc. Am. Bull.* **124**, 400–414 (2012).
22. D. C. J. D. Hoyal, B. A. Sheets, Morphodynamic evolution of experimental cohesive deltas. *J. Geophys. Res.* **114**, F02009 (2009).
23. B. A. Sheets, T. A. Hickson, C. Paola, Assembling the stratigraphic record: Depositional patterns and time-scales in an experimental alluvial basin. *Basin Res.* **14**, 287–301 (2002).
24. T. Muto, Shoreline autoretreat substantiated in flume experiments. *J. Sediment. Res.* **71**, 246–254 (2001).
25. J. B. Swenson, T. Muto, Response of coastal plain rivers to falling relative sea-level: Allogenic controls on the aggradational phase. *Sedimentology* **54**, 207–221 (2007).
26. J. Martin, B. Sheets, C. Paola, D. Hoyal, Influence of steady base-level rise on channel mobility, shoreline migration, and scaling properties of a cohesive experimental delta. *J. Geophys. Res.* **114**, F03017 (2009).
27. H. H. Chang, Fluvial hydraulics of deltas and alluvial fans. *J. Hydr. Div.-ASCE* **108**, 1282–1295 (1982).
28. R. L. Slingerland, J. W. Harbaugh, K. Furlong, *Simulating Clastic Sedimentary Basins* (Prentice Hall, Englewood Cliffs, NJ, 1994).
29. R. S. Snow, R. L. Slingerland, Mathematical modeling of graded river profiles. *J. Geol.* **95**, 15–33 (1987).
30. P. Chatanantavet, M. P. Lamb, Sediment transport and topographic evolution of a coupled river and river plume system: An experimental and numerical study. *J. Geophys. Res.* **119**, 1263–1282 (2014).
31. D. J. Jerolmack, D. Mohrig, Conditions for branching in depositional rivers. *Geology* **35**, 463–466 (2007).
32. K. L. Miller, W. Kim, Laboratory investigation of effects of flood intermittency on river delta dynamics, paper presented at the *AGU Fall Meeting*, San Francisco, CA, 2015.
33. M. D. Reitz, J. L. Pickering, S. L. Goodbred, C. Paola, M. S. Stecker, L. Seeber, S. H. Akhter, Effects of tectonic deformation and sea level on river path selection: Theory and application to the Ganges-Brahmaputra-Meghna River Delta. *J. Geophys. Res.* **120**, 671–689 (2015).
34. D. A. Edmonds, R. L. Slingerland, Significant effect of sediment cohesion on delta morphology. *Nat. Geosci.* **3**, 105–109 (2010).
35. J. H. Nienhuis, A. D. Ashton, L. Giosan, What makes a delta wave-dominated? *Geology* **43**, 511 (2015).
36. M. D. Reitz, D. J. Jerolmack, Experimental alluvial fan evolution: Channel dynamics, slope controls, and shoreline growth. *J. Geophys. Res.* **117**, F02021 (2012).
37. D. Mohrig, P. L. Heller, C. Paola, W. J. Lyons, Interpreting avulsion process from ancient alluvial sequences: Guadalope-Matarranya system (northern Spain) and Wasatch Formation (western Colorado). *Geol. Soc. Am. Bull.* **112**, 1787–1803 (2000).
38. E. A. Hajek, P. L. Heller, E. L. Schur, Field test of autogenic control on alluvial stratigraphy (Ferris Formation, Upper Cretaceous–Paleogene, Wyoming). *Geol. Soc. Am. Bull.* **124**, 1898–1912 (2012).
39. E. A. Hajek, M. A. Wolinsky, Simplified process modeling of river avulsions and alluvial architecture: Connecting models and field data. *Sediment. Geol.* **257–260**, 1–30 (2012).
40. D. A. Edmonds, D. C. J. D. Hoyal, B. A. Sheets, R. L. Slingerland, Predicting delta avulsions: Implications for coastal wetland restoration. *Geology* **37**, 759–762 (2009).
41. L. B. Leopold, T. Maddock Jr., *The Hydraulic Geometry of Stream Channels and Some Physiographic Implications (Geological Survey Professional Paper 252)* (U.S. Government Printing Office, Washington, DC, (1953), 57 pp.
42. G. Parker, P. Wilcock, C. Paola, W. E. Dietrich, J. Pitlick, Physical basis for quasi-universal relations describing bankfull hydraulic geometry of single-thread gravel bed rivers. *J. Geophys. Res.* **112**, F04005 (2007).
43. A. Aslan, W. J. Autin, Evolution of the Holocene Mississippi River floodplain, Ferriday, Louisiana: Insights on the origin of fine-grained floodplains. *J. Sediment. Res.* **69**, 800–815 (1999).
44. W. Kim, D. Mohrig, R. Twilley, C. Paola, G. Parker, Is it feasible to build new land in the Mississippi River Delta? *EOS* **90**, 373–374 (2009).
45. C. Paola, J. M. Martin, Mass-balance effects in depositional systems. *J. Sediment. Res.* **82**, 435–450 (2012).
46. C. Paola, R. R. Twilley, D. A. Edmonds, W. Kim, D. Mohrig, G. Parker, E. Viparelli, V. R. Voller, Natural processes in delta restoration: Application to the Mississippi Delta. *Annu. Rev. Mater. Sci.* **3**, 67–91 (2011).
47. R. J. Russell, R. D. Russell, in *Recent Marine Sediments: A Symposium* (American Association of Petroleum Geologists, Tulsa, OK, 1939), pp. 153–177.

48. G. K. Gilbert, The topographic features of lake shores. *U.S. Geol. Survey Annu. Rep.* **5**, 75–123 (1855).
49. D. A. Edmonds, J. B. Shaw, D. Mohrig, Topset-dominated deltas: A new model for river delta stratigraphy. *Geology* **39**, 1175–1178 (2011).
50. E. W. Lane, *A Study of the Shape of Channels Formed by Natural Streams Flowing in Erodible Material* (U.S. Army Engineer Division, Missouri River, Corps of Engineers, Omaha, NE, 1957).
51. V. T. Chow, *Open-Channel Hydraulics* (McGraw-Hill, New York, 1959).
52. J. C. Rowland, W. E. Dietrich, M. T. Stacey, Morphodynamics of subaqueous levee formation: Insights into river mouth morphologies arising from experiments. *J. Geophys. Res.* **115**, F04007 (2010).
53. G. Parker, *1D Sediment Transport Morphodynamics with Applications to Rivers and Turbidity Currents;* http://hydrolab.illinois.edu/people/parkerg/morphodynamics_e-book.htm.
54. J. A. C. Bresse, Cours de Mecanique Appliquee, Hydraulique (Mallet-Bachelier, Paris, 1860).

Acknowledgments: Critical and constructive comments from C. Paola, D. Mohrig, K. Whipple, D. Edmonds, and D. Jerolmack on an earlier draft improved the presentation of this work. **Funding:** We acknowledge support from NSF (grants OCE-1233685 and 1427177) and the California Institute Technology Terrestrial Hazards Observations and Reporting Center program made possible by Foster and Coco Stanback. V.G. acknowledges further support from National Center for Earth-Surface Dynamics 2 synthesis postdoctoral fellowship and the Imperial College London Junior Research Fellowship. **Author contributions:** M.P.L. and V.G. conceived the study and designed the experiments. All authors helped perform the experiments and analyze the data. V.G. and M.P.L. wrote the paper with input from other authors. **Competing interests:** The authors declare that they have no competing interests. **Data and materials availability:** All data needed to evaluate the conclusions in the paper are present in the paper and/or the Supplementary Materials. Additional data related to this paper are available upon request from V.G. and A.J.C.

Submitted 4 December 2015
Accepted 26 April 2016
Published 20 May 2016
10.1126/sciadv.1501768

Citation: V. Ganti, A. J. Chadwick, H. J. Hassenruck-Gudipati, B. M. Fuller, M. P. Lamb, Experimental river delta size set by multiple floods and backwater hydrodynamics. *Sci. Adv.* **2**, e1501768 (2016).

ScienceAdvances
AAAS

Experimental river delta size set by multiple floods and backwater hydrodynamics

Vamsi Ganti, Austin J. Chadwick, Hima J. Hassenruck-Gudipati, Brian M. Fuller and Michael P. Lamb (May 20, 2016)

Sci Adv 2016, 2:.
doi: 10.1126/sciadv.1501768